Comparative analysis of the follicular transcriptome of Zhedong white geese (*Anser Cygnoides*) with different photoperiods

Zhongbao Xu,[*] Siying Chen,[*] Weihu Chen,[†] Xiaolong Zhou,[*] Feifei Yan,[*] Tao Huang,[*] Yaqin Wang,[‡] Huangda Lu,[§] and Ayong Zhao[*,1]

[*]*College of Animal Sciences and Veterinary Medicine, Zhejiang A&F University, Hangzhou 311300, China;* [†]*Agricultural and Rural Bureau of Xiangshan County, Ningbo 315000, China;* [‡]*Ningbo Agricultural Machinery Animal Husbandry Center, Ningbo 315099, China; and* [§]*NingboTech University, Ningbo 315000, China*

ABSTRACT The laying performance of geese is mainly determined by follicular development and atresia, while follicular status is regulated by photoperiod. To understand the effect of photoperiod on the development of goose follicles, artificial light was used to change the photoperiod. In this study, ten healthy 220-day-old Zhedong white geese (*Anser Cygnoides*) with similar body weights and similar reproductive start times were reared for 60 days under long photoperiod (15 L:9 D) and short photoperiod (9 L:15 D) artificial light with the intensity controlled at 30 lux, and follicles were collected. Follicle development was analyzed by observing the morphology of follicle tissue, the localization of autophagosomes and autolysosomes, and the expression levels of apoptosis-related protein factors. Small white follicles (**SWFs**) were selected for RNA sequencing and bioinformatics analysis of the transcriptome. Under a long photoperiod, microtubule-associated protein 1 light chain 3 (**LC3**) and Caspase-3 were expressed in the granulosa cell layer and oocytes, respectively. LC3 and Caspase-3 protein expression was increased in SWF and large white follicles (**LWFs**), and there were more autophagosomes and autolysosomes in granulosa cells. RNA-seq found 93 differentially expressed genes (**DEGs**) in the short-photoperiod group, including 55 upregulated DEGs and 38 downregulated DEGs, distributed in 37 gene ontology categories. Kyoto Encyclopedia of Genes and Genomes-enriched signaling pathways revealed 5 pathways enriched in upregulated DEGs, including protein digestion and absorption, ECM-receptor interaction and regulation of lipolysis in adipocytes, and 4 pathways enriched in downregulated DEGs, such as fatty acid biosynthesis. Ten differentially expressed genes related to extracellular matrix and fatty acid metabolism (*THBS2, COL12A1, MRC2, TUBA, COL1A1, COL11A1, HSPG2, FABP, MGLL*, and *OLAH*) may be involved in the photoperiod regulation of follicle development in Zhedong white geese. The differentially expressed genes screened in this study will provide new ideas to further understand the molecular mechanism underlying photoperiod-mediated regulation of follicle development in Zhedong white geese.

Key words: SWF, Zhedong white goose, photoperiod, transcriptome

2022 Poultry Science 101:102060
https://doi.org/10.1016/j.psj.2022.102060

INTRODUCTION

Light is one of the most important factors causing seasonal reproduction in animals, and the seasonal variation in the amount of light per day is the most important signal for determining the correct time of year to breed. This biological response to the relative length of day and night is known as photoperiodism (Zhao et al., 2020). The photoperiod of birds was reported for the first time in 1925, and the response of dark-eyed junco (a nontropical bird) gonad development to photoperiod changes was confirmed (Rowan, 1925). Birds depend on seasonal variations in the photoperiod to determine the timing and duration of the breeding season. Birds living in temperate zones are usually long-day breeders, while those living in the tropics or subtropics are short-day breeders (Shi et al., 2008).

The reproductive behavior of poultry is mainly regulated by the hypothalamic-pituitary-gonadal axis. Light stimulation is sensed in deep brain photoreceptors (**DBPs**) (Nakane et al., 2010; Yamashita et al., 2010), and the resulting nerve signals are transmitted to the pituitary nodule (**PT**) to induce the synthesis of thyrotropin, which in turn induces the synthesis of iodomethyronine deiodase Ⅱ (**DiO2**). DiO2 converts thyroxine

Received July 16, 2021.
Accepted September 24, 2021.

[1]Corresponding author: zay503@zafu.edu.cn

(**T4**) to 3,5,3-triiodothyronine (**T3**) in MBH, leading to the synthesis and release of gonadotropin-releasing hormone (**GnRH**) (Yoshimura, 2013; Bédécarrats et al., 2016), which is delivered to the anterior pituitary through the portal vein blood circulation, stimulating the synthesis and release of gonadotropins, luteinizing hormone (**LH**), and follicle-stimulating hormone (**FSH**). LH and FSH promote gonadal maturation and follicle selection and regulate the secretion of regulatory steroids (Leska and Dusza, 2007). The secretion of vasoactive intestinal peptides (**VIPs**) and prolactin (**PRL**), as well as the abundance of mRNAs of these factors, are sensitive to increased photoperiod sensitivity (Mauro et al., 1992; Deviche et al., 2000). In addition, VIP and PRL contribute to the development of photorefractoriness and the inhibition of GnRH and LH secretion.

The phenomenon in which a follicle enters a degenerative process is called follicular atresia. When follicles enter atresia, they do not continue to develop to the next stage, and during the whole stage of follicular development, small follicles are more prone to atresia than preovulatory follicles (Lin and Rui, 2010). The direct cause of follicular atresia is autophagy-induced apoptosis of granulosa cells (Tilly et al., 1991; Markström et al., 2002). Under physiological conditions, apoptosis depends on caspases, while autophagy is carried out through autophagosomes and autophagosolysosomes (Klionsky, 2005; Lockshin and Zakeri, 2005). It was found that rat granulosa cells induced apoptotic cell death through aggregated autophagosomes and caspases (Choi et al., 2010). The expression level of Caspase-3 is higher in the cells of fish atretic follicles (Morais et al., 2012). Microtubule-associated protein 1 light chain 3 (**LC3**) is a marker of autophagosomes (Wu et al., 2006), and its role in follicular atresia has been elucidated by increasing evidence (Zhou et al., 2019). LC3 was upregulated and induced autophagy in mouse granulosa cells caused by tobacco smoke induction (Gannon et al., 2012). In addition, the expression level of LC3 was upregulated during reactive oxygen species (**ROS**) activation of autophagy in goose granulosa cells through the mTOR pathway (Lou et al., 2017).

Zhedong white goose (*Anser Cygnoides*), mainly distributed in the eastern Zhejiang Province of China is a famous local breed of meat goose in China. However, it has strict seasonal reproduction, a high tendency toward broodiness and a low egg-laying rate (Zhao et al., 2013). Artificial light can control the reproductive behavior of geese so that the photorefractoriness of geese is delayed and geese are induced to lay eggs out of season (Buckland and Guy, 2002; Shi et al., 2005). Previous studies exposed egg-laying Zhedong white geese to both a short photoperiod (9 L:15 D) and a long photoperiod (15 L:9 D) (when natural light was 10.5−11 h). A short photoperiod produces more eggs than a long photoperiod and makes geese finish nesting earlier and resume laying eggs (Chen et al., 2020). In this study, the expression of the autophagy factors LC3 and Caspase-3 in small white follicles (**SWFs**) was detected by immunohistochemistry and Western blot, and SWF autophagosomes and autophagosolysosomes were observed by transmission electron microscopy to investigate autophagy in SWFs. Transcriptome analysis was used to study the differentially expressed genes of SWF in Zhedong white geese to explore the regulation of light duration in breeding season on follicular development and follicular atresia.

MATERIALS AND METHODS

Ethics Statement

In this study, all experimental protocols relating to animal experiments were in accordance with the measures of the Administration of Affairs Concerning Experimental Animals of Zhejiang Province, China (approved by the Zhejiang Provincial Government in 2009 and promulgated by Decree No. 263). All animal experiments in this study were approved by the Animal Care and Use Committee of Zhejiang A&F University (Lin'an, Zhejiang, China) to ensure compliance with international animal welfare guidelines.

Animals, Feeding, and Sample Collection

Zhedong white geese (*A. Cygnoides*) used in this study were raised in East Zhejiang White Goose Original Breeding Farm, Xiangshan County, Zhejiang Province, China. Twenty healthy and normal Zhedong white geese with similar body weights and reproduction start times were randomly selected. They were randomly divided into 2 groups, with 10 birds in each group, according to normal feeding and management methods. Two groups of geese entering the laying period (220 d of age) were reared under long photoperiod (15 L:9 D) and short photoperiod (9 L:15 D) artificial light, the intensity of which was controlled at 30 lux. Both groups stopped laying eggs at wk 6, but the short-photoperiod group resumed laying eggs at wk 8. After 60 days of feeding, 6 geese in each group were dissected, and all follicles were collected and graded according to volume. After all levels of follicles were counted, they were immediately frozen in liquid nitrogen and stored at −80°C until use. Three geese were selected from each group, and 4 SWFs from each goose were randomly selected and immersed in a 2 mL centrifuge tube filled with 2.5% Gluta fixation solution and 4% paraformaldehyde.

Follicular Granulosa Cell Autophagy Observations

The follicle tissue was soaked in 2.5% Gluta fixation liquid (exclusive use for electron microscopy) (Solarbio, Beijing, China). This was followed by fixation in 1% osmium acid solution, dehydration in gradient concentration ethanol solutions and embedding in spurr embedding agent. Seventy- to 90-nm slices were prepared by an ultrathin microslicer (Leica EM UC7, Wetzlar, Germany) and stained with lead citrate solution and 50% ethanol saturated solution of uranium dioxide

acetate. Ultrastructure images were captured using transmission electron microscopy (Hitachi H-7650, Tokyo, Japan). There were three samples from each group of 3 geese, and 3 micrographs were taken with systematic random sampling from each sample. The mean value of data from each group of 9 micrographs was used for quantitative statistics.

Immunohistochemistry

Paraffin-embedded sections of SWFs were dewaxed in xylene, rehydrated in a graded ethanol series and finally rinsed with phosphate-buffered saline (**PBS**). This was followed by incubation in citrate antigen repair buffer at 100°C, and the endogenous enzymes were inactivated with 3% H2O2-methanol solution. The slices were incubated in a humidified chamber with 1:100 dilutions of Caspase-3 antibody (A16793, ABclonal, Wuhan, China) or LC3 antibody (A19665, ABclonal, Wuhan, China), strengthening agent and horseradish peroxidase (**HRP**)-conjugated immunoglobulin G (KIT-9902, MXB Biotechnologies, Fuzhou, China) successively. After washing thoroughly, the slices were stained with a DAB kit (DAB-1031, MXB Biotechnologies, Fuzhou, China) and subsequently counterstained with hematoxylin. After dehydration, the slices were sealed with neutral resin and observed under a light microscope.

Analysis of LC3 Protein Expression in Follicles

Follicular lysates were prepared using cold RIPA buffer containing protease inhibitors, phosphatase inhibitors and PMSF. Protein concentration was determined using a BCA Protein Detection Kit (Jiancheng Institute of Biological Engineering, Nanjing, China). An equal amount of protein was loaded onto a 12% SDS−PAGE gel separated by electrophoresis and transferred to PVDF membranes. After blocking with 5% skimmed milk powder, Western blotting was performed with LC3 antibody (AbClonal, Wuhan, China) and horseradish peroxidase-conjugated goat anti-rabbit antibody (Abbkine, Wuhan, China). The PVDF membrane was exposed and photographed in an agglutination imaging system using Western Chemiluminescent HRP Substrate (Millipore, Boston) according to the operating instructions. The band strength was quantified using ImageJ software, and the results were normalized to β-tubulin.

Construction and Sequencing of mRNA Library

SWFs were delivered to Shanghai Majorbio Biopharm Technology Co., Ltd. (Shanghai, China) for RNA extraction and sequencing. Total RNA was extracted from tissue samples, and the concentration and purity of the extracted RNA were detected by a NanoDrop2000. RNA integrity was detected by agarose gel electrophoresis, and the RIN value was determined by an Agilent 2100. The total amount, concentration, OD260/280 and OD260/230 of RNA should be equal to or greater than 1 μg, 35 ng/μL, 1.8, and ≥1.0, respectively, for single database construction. The RNA fragments were constructed into cDNA libraries according to the protocol of the Illumina TruSeqTM RNA Sample Prep Kit (Illumina, San Diego, CA). According to the protocol recommended by the supplier, libraries were sequenced on the Illumina NovaSeq 6000 platform.

RNA-seq Data Analysis

Clean reads were obtained by deleting reads containing Adapter, Poly-N, and low-quality reads from the original data. Via TopHat software, the clean reads were mapped to the NCBI TopHat *Anser cygnoides* domesticus reference genome (https://www.ncbi.nlm.nih.gov/genome/31397? Genome_Assembly_id = 229313). Transcripts were assembled, and the abundance was measured via Cufflinks. Gene expression levels were estimated using fragments per kilobase million (**FPKM**). Differentially expressed genes (**DEGs**) were analyzed through DESeq2 software (http://bioconductor.org/packages/stats/bioc/DESeq2/). When |log2FC| was greater than 1 and *P*-adjusted was less than 0.0001, the gene expression level was considered to be significantly different.

Function Annotation for DEGs

Gene Ontology (**GO**) analysis of DEGs was carried out using the GeneOntology database (http://www.geneontology.org/). GO enrichment analysis was used to analyze the main functions of DEGs. DEGs were annotated from 3 definitions, including biological processes, molecular functions, and cellular components. P values < 0.05 were defined as the significantly enriched GO terms associated with DEGs. KEGG (Kyoto Encyclopedia of Genes and Genomes) pathway analysis was performed using the KEGG database to identify important pathways involved in DEGs. P values < 0.02 were used to define significantly enriched KEGG pathways.

Real-Time Quantitative PCR Validation

To determine transcriptome sequencing data, 10 candidate genes were selected and validated by qRT-PCR. The primers for qRT-PCR were designed using Primer Premier 5 software and synthesized by Hangzhou Youkang Biotechnology Co., Ltd. (Hangzhou, China). The primer information is listed in Table 1. RNA from tissues was used to synthesize cDNA using a 5X All-in-One Mastermix Kit (ABM, Vancouver, Canada) and as a template for quantitative PCR. Glyceraldehyde-3-phosphate dehydrogenase (**GAPDH**) was used as an internal control. Each 10 μL reaction volume contained 5 μL of 2X TB Green Premix Ex Taq (Takara, Kyoto, Japan), 0.2 μL of 10 μM forward and reverse primers, 1

Table 1. Primers used in the real-time quantitative PCR assay of genes.

Gene name	Forward primer sequence (5'-3')	Reverse primer sequence (5'-3')	PCR product (bp)
GADPH	TTCCTCCACCTTTGATGCGG	ACCATCAAGTCCACCACACG	114
MRC2	TGGGACGGCGAGTATTTCTG	GCCCTTATTGTAACCGGGCT	126
HSPG2	AGGTGTCAGTGGCTGATTCG	AGGGGAGTAGTAGGTGCCAG	116
COL11A1	GCATCGAGTAGCCATTAGCG	CTTTCCAGGGGTTTTGTA GTTTT	84
MGLL	GAGTCCTCAAAACATCCCGTACA	TTGTTGCTGGCTTCCAATACC	92
TUBA	TGAGCTGTGGAGGGACGC	GGGAAGTGGATGTAGGGGTATG	80
COL1A	GTTGATAGCAGCGACTGTACTACTCA	TGGCAGGGCTCGGGTT	123
THBS2	CTCTTTTGTTCAACCCTCGTCA	TCACCCTCCCCATTATTATCTGT	121
COL12A1	AGCAACCCACTTGTTGGACA	CATCCACCAGCAGCACGATA	121
FABP	GAGACCACAGCAGATGACAGAA	ATTCCACGACCAGGTTCCCA	136

μL of cDNA, and 3.6 μL of RNA-free water. qRT-PCR was performed on a CFX96 Real-time System (Bio-Rad, Hercules, California) as follows: a cycle at 95°C for 30 s, followed by 40 cycles of 95°C denaturation at 5 s and annealing at 60°C for 30 s. There were 3 replicates for each sample. The relative expression levels of the related genes were calculated using the $2^{-\Delta\Delta CT}$ statistical analysis method, and the long-photoperiod group served as the calibrator.

Statistical Analysis

All experiments were repeated at least 3 times. Data were analyzed by independent samples t test using IBM SPSS statistics 22 software, graphed using GraphPad Prism software and presented as the mean ± SEM. $P < 0.05$ was considered to be statistically significant. $P < 0.01$ was considered to be very statistically significant.

RESULTS

The Histological Morphology of Follicles

The ovarian development of Zhedong white geese with a short photoperiod was normal, and there were large numbers of developing follicles at all levels, which formed follicular growth waves. In addition, there were several preovulatory follicles. Most of the follicles were fully developed and bright in color and luster (Figure 1A). Ovarian atrophy with a long photoperiod showed no preovulatory follicles and only pregrade follicles, and most of them were SWF. Most of the follicles were atresic and dark in color and luster, and some of the follicles also had blood spots. There was no significant difference in the number of SWFs and LWFs between the 2 groups ($P > 0.05$), but the SYF number of a short photoperiod was significantly higher than that of a long photoperiod ($P < 0.05$; Figure 1B).

Follicular Granulosa Cell Autolysosomes and Autophagosomes

There were autophagosomes and autolysosomes in the fields of vision for the vesicle granulosa cell layer. Autophagosomes are vesicular structures with bilayer membranes with diameters of 300 to 900 nm that encase other cellular components or organelles. Autolysosomes are monolayer vesicular structures containing cytoplasmic components that are not completely degraded (Figure 2A). Calculated as the average of the number in each group of nine images, the number of autophagosomes and autolysosomes in the granulosa cell layer of

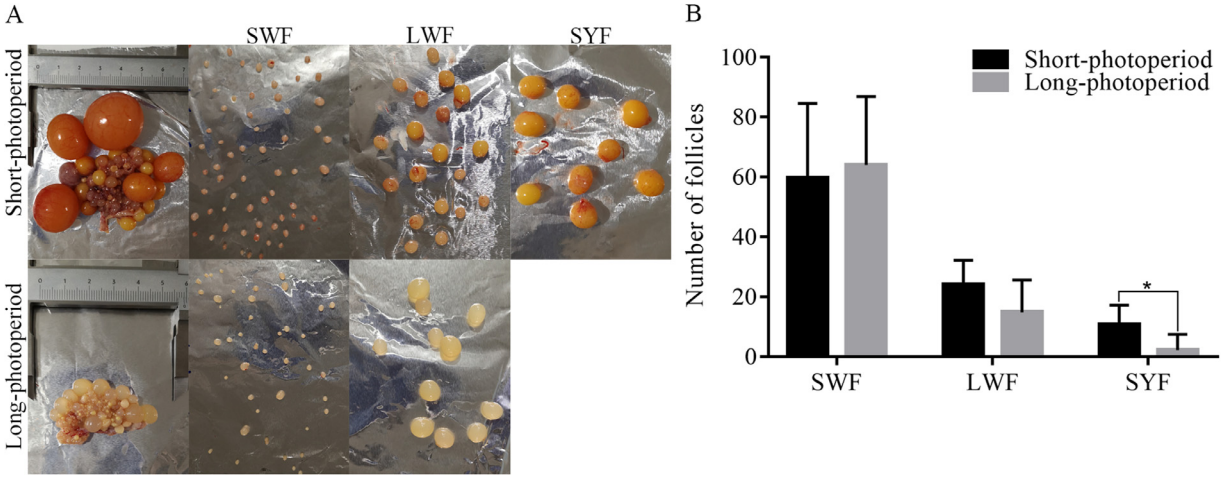

Figure 1. Follicles of Zhedong White geese in the two groups. (A) Ovarian follicle anatomy. SWF, LWF, and SYF represent small white follicles, large white follicles, and small yellow follicles, respectively. (B) Number of follicles. Values are mean ± SEM (n = 6). "*" indicates significant differences between groups ($P < 0.05$).

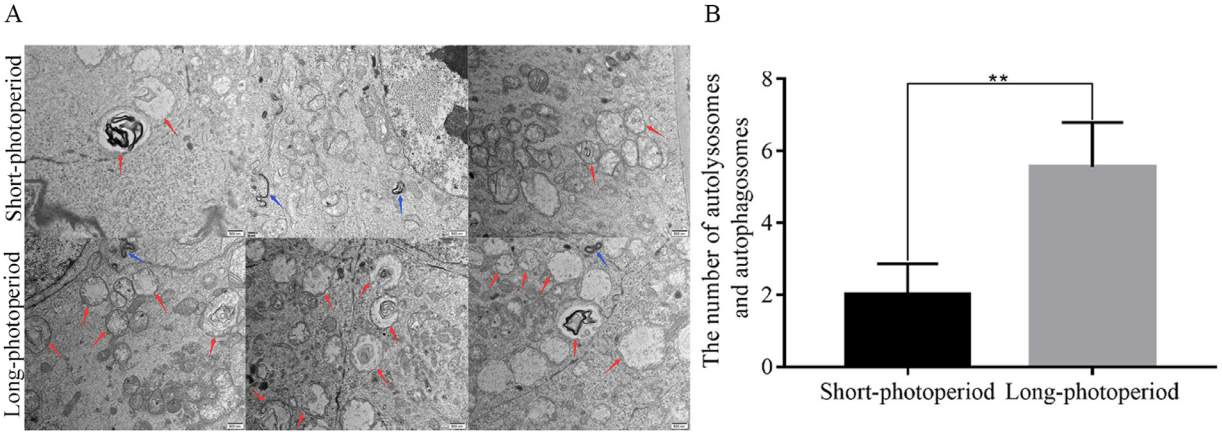

Figure 2. Autophagy in the follicular granule layer of Zhedong White geese. (A) Electron microscopic observation of autophagosomes and autophagolysosomes. The red and blue arrows point to autolysosomes and autophagosomes, respectively. Scale bar = 500 nm. (B) The number of autophagosomes and autophagosomes. Values are mean ± SEM (n = 9). "**" indicates highly significant differences between groups ($P < 0.01$).

follicles with a long photoperiod was significantly higher than that of follicles with a short photoperiod (Figure 2B).

Immunohistochemistry

LC3 protein was mainly expressed in the follicular granulosa cell layer with a long photoperiod (shown as brown in the figure) and was almost never expressed in the oocyte and membrane layer with a long photoperiod or in the follicle with a short photoperiod. Caspase-3 protein was barely expressed in SWFs in either group (Figure 3A).

Analysis of LC3 Protein Expression in Follicles

The relative expression of LC3 protein relative to the reference protein β-tubulin in SWFs and LWFs was detected by Western blot. The relative expression level of LC3II protein in SWFs and LWFs with a long photoperiod was significantly higher than that with a short photoperiod ($P < 0.05$; Figure 3B).

Transcriptome Sequencing and Quality Control

A SWF library of Zhedong white geese treated with different photoperiods was constructed and sequenced. Each library generated a total of 46,735,288 to 51,248,378 original reads, and the effective data were 46250,628 to 50814222 reads, with an effective ratio of 6 libraries greater than 98.9%. The data quality was good, with Q20 (base sequencing error probability <1%) >97.9% and Q30 (base sequencing error probability <0.1%) >94.0% (Table 2).

Reads Mapping and DEGs

To identify the genes corresponding to clean reads in each library, clean reads were mapped to the reference gene expressed in the genome of *Anser cygnoides* domesticus. The mapping results showed that 83.73% to 86.42% reads in each library were completely matched with the reference genome, while 80.51% (37,240,075) to 84.18% (42,781,369) reads among unique mapping reads were completely matched with

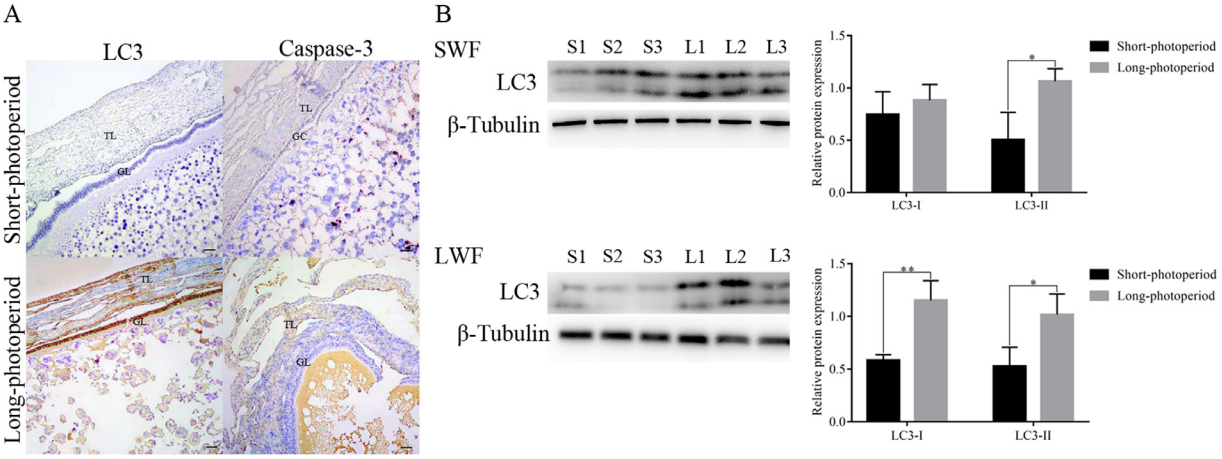

Figure 3. Expression of LC3 and Caspase-3 in follicles. (A) Immunolocalization of LC3 and Caspase-3 protein in small white follicles (SWFs). GL and TL represent the oocyte, granulosa cell layer, and theca cell layer, respectively. Scale bar = 40 μm. (B) Western blot analysis of LC3 expression in SWF and large white follicles (LWFs). Values are mean ± SEM (n = 3). "*" and "**" indicate significant and highly significant differences between groups, respectively ($P < 0.05$).

Table 2. Characteristics of the reads from 6 samples in Zhedong white geese.

Sample	Raw data		Valid data		Valid ratio (%)	Q20 (%)	Q30 (%)
	Reads	Base	Reads	Base			
L1	49371444	7455088044	48955774	7269402282	99.16	98.12	94.54
L2	51248378	7738505078	50814222	7529671916	99.15	98.14	94.61
L3	50521606	7628762506	50072374	7460074066	99.11	98.05	94.36
S1	46735288	7057028488	46250628	6892220180	98.96	97.97	94.24
S2	48929738	7388390438	48467798	7241169726	99.06	97.99	94.24
S3	50498222	7625231522	50051462	7485099560	99.12	97.98	94.19

L and S represent the long-photoperiod group and the short-photoperiod group, respectively; 1/2/3 represent three biological replicates of each group; Raw data: all original data produced by sequencing; Valid reads: the remaining reads after filtering of low-quality reads from raw reads; Valid ratio: Ratio of valid reads to raw reads; Q20: the proportion of read bases whose error rate is less than 1%; Q30: the proportion of read bases whose error rate is less than 0.1%.

Table 3. Mapped statistical results of 6 libraries.

Sample	Total reads	Total mapped	Multiple mapped	Uniquely mapped
L1	48961268	41848824(85.47%)	845995(1.73%)	41002829(83.75%)
L2	50819934	43919821(86.42%)	1138452(2.24%)	42781369(84.18%)
L3	50077710	42971146(85.81%)	912136(1.82%)	42059010(83.99%)
S1	46257872	38733175(83.73%)	1493100(3.23%)	37240075(80.51%)
S2	48472522	41178968(84.95%)	1059799(2.19%)	40119169(82.77%)
S3	50057182	42743945(85.39%)	1455954(2.91%)	41287991(82.48%)

L and S represent the long-photoperiod group and the short-photoperiod group, respectively; 1/2/3 represent three biological replicates of each group; Total reads: the remaining reads after filtering of low-quality reads from raw reads (i.e., Valid reads); Total mapped: the total reads amount mapped to the reference genome; Multiple mapped: the reads amount mapped to the reference genome at more than one site; Uniquely mapped: the reads amount mapped to the reference genome at only one site.

the reference genome, and 1.73% (845,995) to 3.23% (1,493,100) reads among multimapping reads were completely matched with the reference genome (Table 3). We identified 93 differentially expressed genes in the SWF library (P-adjust < 0.0001 and | log2FC|≥1), which contained 55 upregulated genes and 38 downregulated genes (Figure 4).

GO and KEGG Pathway Analyses of DEGs

To determine the functions of DEGs, GO enrichment analysis was used to annotate DEGs, and their distribution was studied. Ninety-three differentially expressed genes were distributed in 37 gene ontology categories, which were divided into 3 categories: biological processes, cell components, and molecular functions, accounting for 48.6, 32.4, and 19.0%, respectively (Figures 5A−5B). Among them, the most important biological processes include cellular processes, single-organism processes, metabolic processes, biological regulation, and regulation of biological processes. In terms of cell composition, genes participate in cell, organelle, extracellular region, extracellular region part, etc. In the classification of molecular functions, enriched GO terms included binding, catalytic activity, transporter activity, structural molecule activity, etc.

To understand the regulatory network of DEGs by comparing the transcriptome of SWFs exposed to different photoperiods in the 2 groups, KEGG pathway enrichment analysis was performed. In the KEGG pathway analysis of SWF, 93 DEGs were mapped to 94 pathways (Figure 5C).

The upregulated genes were significantly enriched in 5 KEGG pathways, including phagosome, protein digestion and absorption, tuberculosis, ECM-receptor interaction, and regulation of lipolysis in adipocytes. The downregulated genes were significantly enriched in 4 KEGG pathways, including fatty acid biosynthesis, apoptosis, alcoholism, and systemic lupus erythematosus (P value < 0.02; Figure 5D).

qRT−PCR Validation of Gene Expression

To evaluate the accuracy of the RNA-seq data, 10 DEGs were selected for qRT−PCR verification. Although the expression fold changes of the genes selected by the 2 methods were different, the expression trends were highly consistent, which showed the accuracy and quality of the RNA-seq results (Figure 6).

DISCUSSION

Artificial light affects the reproductive performance of poultry, which depends on the growth and development of follicles, strictly following the appropriate hierarchy. After recruitment, the primordial follicles enter grade development, and follicles grow, mature and ovulate in turn from small to large. A large number of primitive follicles are attached to the ovaries of birds, but only a small number of the primitive follicles can grow and mature normally. Only a small percentage of SWFs can

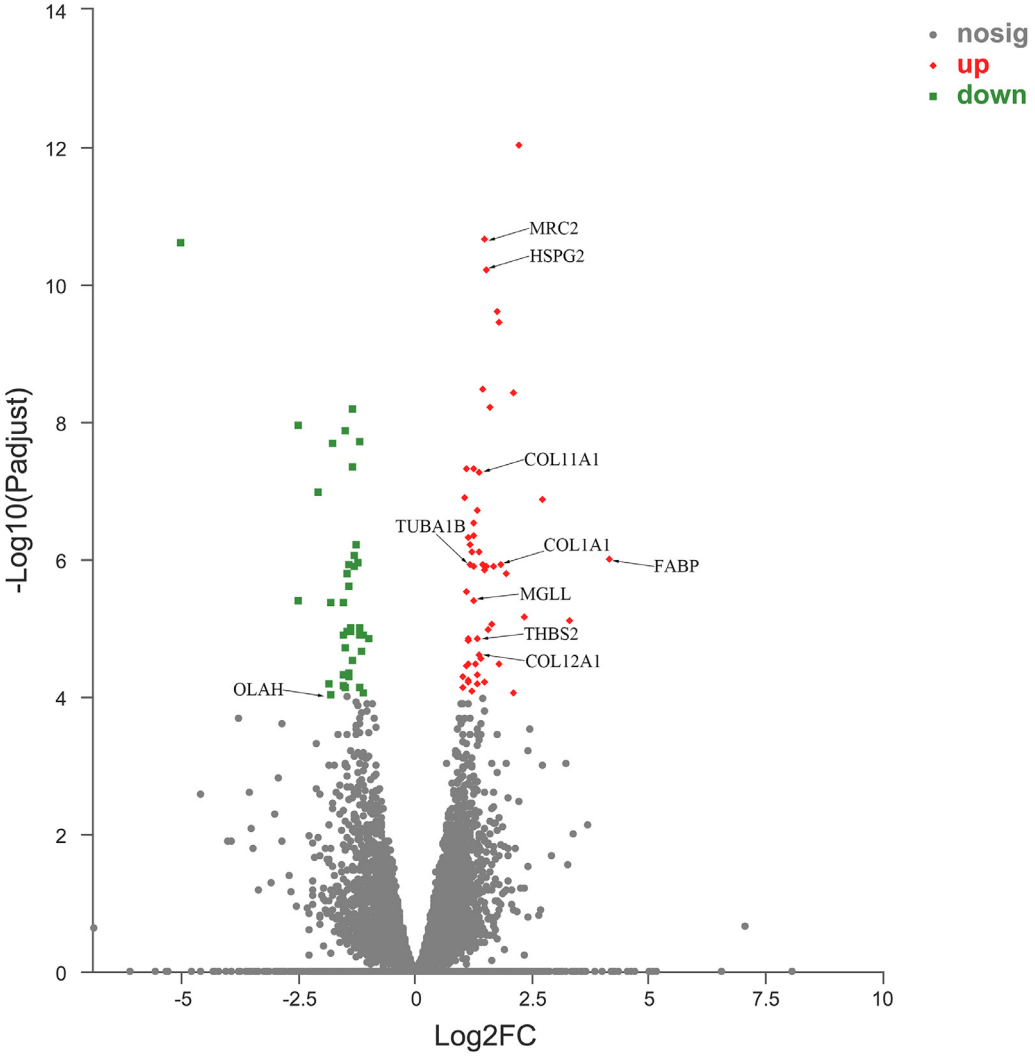

Figure 4. Volcano plot for DEGs.

develop into SYFs, and only one SYF is selected as a graded follicle. The greater the number of follicles selected for grade development, the longer the egg sequence and the higher the egg performance of the bird. We found that a long photoperiod inhibits follicular development by ovarian atrophy and SYF loss in Zhedong white geese. This result is consistent with previous studies showing that a long photoperiod reduced egg production in Zhedong white geese (Chen et al., 2020). Therefore, a short photoperiod is beneficial to follicle development and the laying performance of Zhedong white geese.

Follicular granulosa cell apoptosis, induced by autophagy (Choi et al., 2011), is a direct factor in the occurrence of follicular atresia (Zhang et al., 2019) and is involved in the atresia of various stages of follicular development (Chio et al., 2010). Granulosa cells secrete gonadal steroids, growth factors, and cytokines for follicular growth (Matsuda et al., 2012), so they are the first cell population to undergo apoptosis in follicular atresia and secrete apoptosis-related factors (Inoue et al., 2011). Autophagy, a lysosome-mediated degradation system for maintaining cellular homeostasis, occurs in a stepwise manner involving sequential membrane remodeling processes (Gómez-Sánchez et al., 2021; Zhao et al., 2021). In the autophagy process, cytosolic material is sequestered by an expanding membrane sac (the phagophore), resulting in the formation of a double-membrane vesicle (autophagosome) whose outer membrane subsequently fuses with a lysosome to form a single membrane structure, the autophagy lysosome, exposing the inner single membrane of the autophagosome to lysosomal hydrolases (Xie and Klionsky, 2007). The acidic environment in lysosomes and the action of hydrolases lead to the degradation of autophagy membranes and inclusions (Button et al., 2017). The accumulation of autophagosomes in rat ovarian granulosa cells induces apoptosis of granulosa cells and follicular atresia (Choi et al., 2011). LC3, a widely used autophagic marker, labels autophagic structures at different stages of biogenesis and accumulates on amphisomes during maturation (Zhao et al., 2021). LC3 is necessary for the formation of autophagosomes, during which LC3-I is transformed into LC3-II, LC3-II exists inside and outside the autophagosomes, and its quantity is related to the degree of autophagosome formation (Kabeya et al., 2000; Stolz et al., 2014).

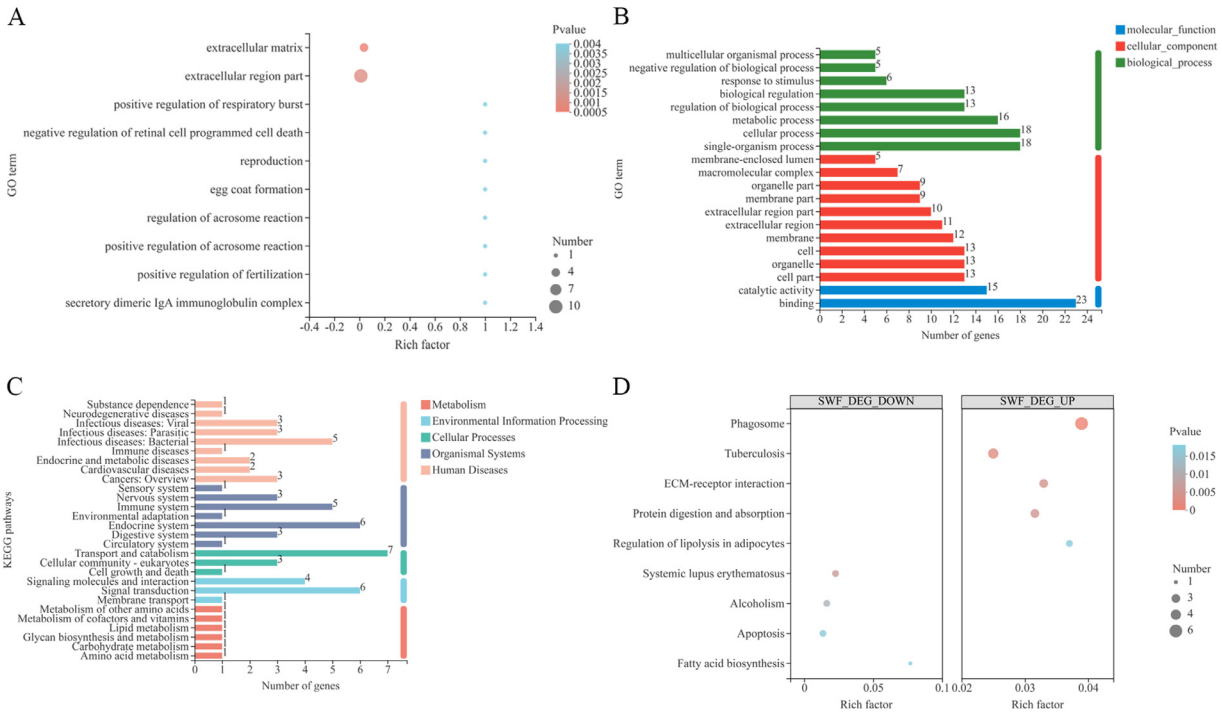

Figure 5. Functional analysis of differentially expressed genes (DEGs) in small white follicles (SWFs). (A) Gene ontology (GO) enrichment analysis of DEGs. The ordinate coordinates represent the annotation of the term; the horizontal axis represents the GO terms corresponding to the rich factor. The rich factor is the ratio of the number of genes enriched in the GO term (sample number) to the number of annotated genes (background number). The higher the Rich factor is, the greater the enrichment degree. The size of the dots indicates the number of genes in this GO term, and the color of the dots corresponds to different P value ranges. (B) GO functional analysis of DEGs. The ordinate coordinates represent three GO categories at the level of the GO term and the annotation of the term; the abscissa is the number of genes. Three different classifications of GO annotations of three basic categories are included (from top to bottom: molecular function, cellular component, and biological processes). (C) Kyoto Encyclopedia of Genes and Genomes (KEGG) pathway functional analysis of DEGs. The vertical axis represents the name of the pathway; the horizontal axis represents the number of genes. Five different classifications of KEGG annotations of six basic categories are included (from top to bottom: metabolism, environmental information processing, cellular processes, organismal systems, and human diseases). (D) Kyoto Encyclopedia of Genes and Genomes (KEGG) pathway enrichment of DEGs. The vertical axis represents the name of the pathway; the horizontal axis represents the pathways corresponding to the rich factor. The rich factor is the ratio of the number of genes enriched in the pathway (sample number) and the number of annotated genes (background number). The higher the Rich factor is, the greater the enrichment degree. The size of the dots indicates the number of genes in this pathway, and the color of the dots corresponds to different *P* value ranges. Among the upregulated and downregulated DEGs, the 5 pathways with the most significant enrichment are displayed in the figure. Abbreviations: SWF_DEG_DOWN: downregulated differential genes in SWF; SWF_DEG_UP: upregulated differential genes in SWF.

This was consistent with the results of this study in which the number of autophagosomes and autophagolysosomes as well as LC3 expression increased in the long photoperiod group, suggesting that a long photoperiod induced follicular atresia through autophagy of follicular granulosa cells and affected egg production in Zhedong white geese. In addition, the major effectors in apoptosis are caspases, which may be involved in later events of autophagy (Santos et al., 2008). The accumulation of autophagosomes induces granulosa cell apoptosis by reducing Caspase-3 (Choi et al., 2011). Our immunohistochemical results also showed that a long photoperiod promotes the accumulation of autophagosomes and autophagolysosomes in SWF granulosa cells of Zhedong white geese to induce cell apoptosis by reducing Caspase-3.

Among the 93 DEGs, we found that *THBS2* and *COL12A1*, partially associated with extracellular matrix and extracellular region, were significantly upregulated in SWFs in the short-photoperiod group. THBS2 (Thrombospondin 2), a member of the thrombospondin family, has binding sites for metal matrix transferases (**MMPs**) and interacts with a variety of cellular receptors, growth factors, and extracellular matrix proteins (Du, 2018). Epithelial cells lose cell polarity and lose their connection with the basement membrane through epithelial mesenchymal transition (**EMT**). THBS2 blocks the EMT process and maintains the epithelial morphology of follicular granulosa cells (Del Pozo Martin et al., 2015). *COL12A1,* encoding the collagen XIIα1 chain, consists of 3 noncollagenous domains and 2 collagenous domains alternating to form a trimer. Collagen XII forms a molecular bridge with tenascin X, which makes the extracellular matrix more resistant to mechanical stress. Collagen XII is upregulated in vitro and in vivo when mechanical stress is applied (Trächslin et al., 1999; Flück et al., 2000). In addition, collagen XII improves the deformability of the matrix and the mobility of collagen fibers, contributing to the elasticity of the extracellular matrix (Nishiyama et al., 1994; Bader et al., 2009). A short photoperiod may improve the elasticity of the extracellular matrix and maintain cell morphology by promoting the expression of the *THBS2* and *COL12A1* genes in the SWF of Zhedong white geese.

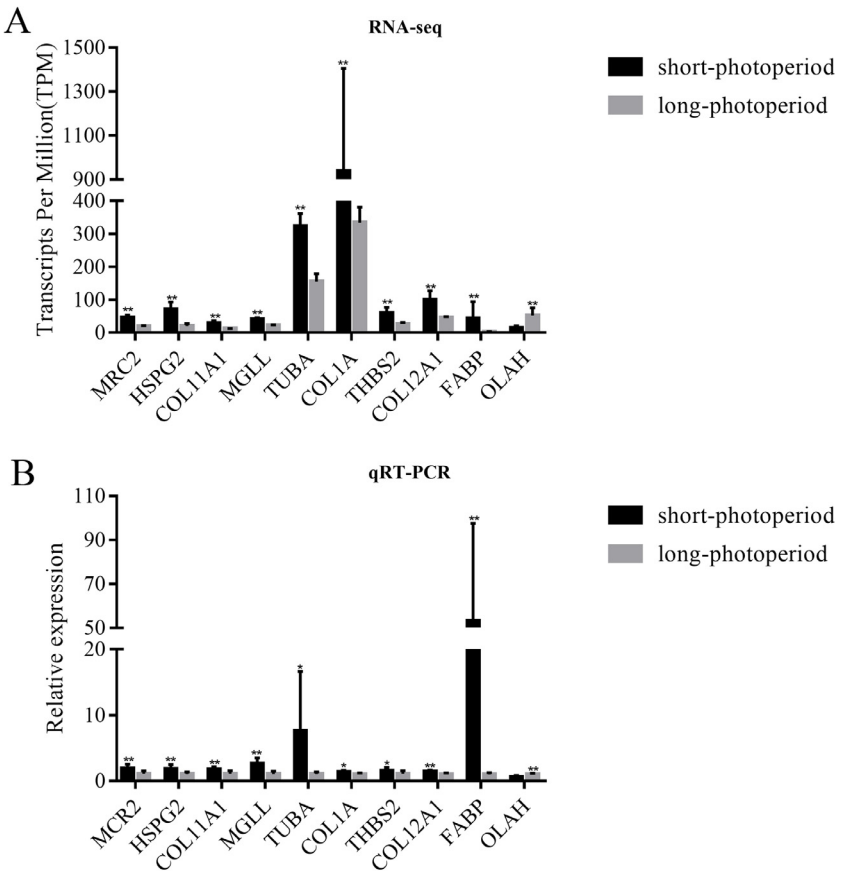

Figure 6. qPCR validation of DEGs by qPCR and RNA-seq results. Total RNA was extracted from SWFs and measured by qRT−PCR analysis; relative expression levels were calculated according to the $2^{-\Delta\Delta Ct}$ method using *GAPDH* as an internal reference gene. Values are mean ± SEM (n = 3). "*" and "**" indicate significant and highly significant differences between groups, respectively ($P < 0.05$). Abbreviations: RNA-seq, RNA sequencing; qPCR. quantitative polymerase chain reaction.

Follicle development requires a large amount of renewal of extracellular matrix components and tissue remodeling to continuously modify the dynamic structure to maintain the homeostasis of the tissue (Yin et al., 2021). In the SWF of Zhedong white geese with a short photoperiod, the phagosome KEGG pathway significantly enriched 6 upregulated DEGs, among which *MCR2* and *TUBA* were associated with extracellular matrix renewal. *MRC2*, also known as uPARAP/Endo180, encodes an endocytic collagen receptor and plays a role in extracellular matrix remodeling by mediating collagen internalization and lysosomal degradation (Howard and Isacke, 2002). It controls the balance of collagen deposition and degradation, mediates the endocytosis pathway of collagen turnover and limits collagen accumulation during fibrogenesis (Madsen et al., 2012). The accumulation of collagen in the outer matrix of hepatocyte pairs leads to liver fibrosis and cirrhosis (Madsen et al., 2012). In addition, *MRC2* was found to be expressed in the TC layer and involved in regulating estradiol synthesis in follicles (Jing et al., 2018). In chicken follicles, TCs and GCs surround oocytes, and interactions between them and between cells and oocytes within the follicle play an important role in follicular genesis, supporting oocyte development until ovulation. In the short-photoperiod group, the upregulation of *MCR2* contributed to the recombination of extracellular matrix of follicles and normal cell growth. α-Tubulin encoded by *TUBA* is an important component of the cytoskeleton and plays a role in cell structure maintenance and material transport (Hong et al., 2017). It was found to be upregulated during the transition from G1 to S phase, which is considered a major checkpoint for cell cycle progression. Increased *TUBA* expression may enhance tumor proliferation (Lu et al., 2013). Collagen is the main component of the extracellular matrix, which consists of 28 subtypes. *COL1A1* and *COL11A1* were found in protein and absorption KEGG pathways enriched with differentially expressed genes upregulated by short photoperiods. *COL1A1* encodes type I collagen α1, the main component of type I collagen, which confers survival advantages and enhanced carcinogenicity to HCC cells (Ma et al., 2019). Silencing of *COL1A1* expression inhibits the proliferation, cloning and motility of HCC cells as well as the formation of tumor spheres. *COL11A1* expression is low in normal tissues but significantly upregulated in many types of cancer (Raglow and Thomas, 2015; Vázquez et al., 2015). *COL11A1* expression was also positively correlated with matrix hardness, disease progression, and extracellular matrix increase. Increased tissue stiffness may alter mechanical transduction, leading to recombination of the extracellular matrix

(Pearce et al., 2017). *COL11A1* activates the Src-PI3K/Akt-NF-kB signaling pathway and induces the expression of 3 antiapoptotic proteins (**IAPs**), including XIAP BIRC2 and BIRC3 (Lu et al, 2013). Therefore, a short photoperiod may promote the renewal and recombination of the extracellular matrix of small white follicles through upregulation of *MCR2, TUBA, COL1A1*, and *COL11A1* to maintain follicular development.

After the oocyte in the primitive follicle is activated and begins to grow, granulosa cells begin to divide, the number of cell layers around the oocyte increases, and the basal membrane of the follicle expands. We found *HSPG2* in the upregulated DEGs enriched by the ECM-receptor interaction pathway, and the Perlecan protein encoded by *HSPG2* is the main component of all basement membranes (Iozzo et al., 1994). It is highly expressed in the external matrix of ovarian cells (Winkler et al., 2002), effectively promotes the activity of growth factors and stimulates the growth and regeneration of endothelial cells (Chen et al., 2008; Mishra et al., 2011; Gustafsson et al., 2013; Grindel et al., 2014). In skeletal muscle, Perlecan causes muscle cell proliferation through growth factor signaling and influences cell stability through integrin B1 (Iozzo et al., 1994).

Follicular development and atresia involve metabolic changes such as sugars and fatty acids, and oocyte maturation depends on the extracellular microenvironment and endogenous substances to maintain energy balance (Sturmey et al., 2009). Triglycerides are the major component of lipids in oocytes (Homa et al., 1986) and provide a large potential energy reserve. The lipase activity of bovine oocytes increases during maturation (Cetica, 2002). In this study, a short photoperiod may promote oxidative metabolism of SWF fatty acids and follicular development by upregulating *FABP* and *MGLL* in the regulation of lipolysis in the adipocyte KEGG pathway. *FABP* is thought to be involved in the uptake, intracellular metabolism, and/or transport of long-chain fatty acids. They may also play a role in regulating cell growth and proliferation. *MGLL* encodes monoglyceride lipase and catalyzes the conversion of monoglycerides to free fatty acids and glycerol. In lipid metabolism, monacylglycerides are converted into fatty acids by hydrolase expressed by *MGLL*, which is bound by FABP and transported to mitochondria, where they enter mitochondria for oxidative decomposition under the action of CPT1. Meanwhile, a short photoperiod may protect oocytes by downregulating *OLAH* in the fatty acid biosynthesis KEGG pathway in SWF, a gene encoding oleacyl-ACP hydrolase, which releases free fatty acids from fatty acid synthase. A decrease in saturated fatty acids in follicular fluid protects oocytes from damage. During follicular atresia, the metabolic level of follicular cells was significantly reduced, and a higher concentration of saturated fatty acids accelerated the apoptosis process of granulosa cells and oocytes (Cheng, 2018).

CONCLUSIONS

In the present study, through follicular morphology, autolysosomes and autophagosomes, as well as the protein expression levels of LC3 and caspase-3, we found that a short photoperiod can inhibit autophagy and follicular atresia and promote follicular development in Zhedong white geese. RNA-seq found that 55 DEGs were upregulated and 38 DEGs were downregulated in the short-photoperiod group. Ten differentially expressed genes related to extracellular matrix and fatty acid metabolism (*THBS2, COL12A1, MRC2, TUBA, COL1A1, COL11A1, HSPG2, FABP MGLL*, and *OLAH*) may be involved in the photoperiod regulation of follicle development in Zhedong white geese. Therefore, our study provides useful information for understanding the photoperiod regulation of follicle development in Zhedong white geese. However, these transcriptome data are preliminary, so the functions of DEGs need to be further investigated.

ACKNOWLEDGMENTS

This study was supported by a grant from the National Natural Science Foundation of China (No. 31872397). The authors are grateful to the Animal Health Research Center of Zhejiang Agriculture and Forestry University for the use of equipment and the Agriculture and Rural Bureau of Xiangshan County for their help.

DISCLOSURES

The authors declare no conflict of interest.

REFERENCES

Bader, H. L., D. R. Keene, B. Charvet, G. Veit, W. Driever, M. Koch, and F. Ruggiero. 2009. Zebrafish collagen XII is present in embryonic connective tissue sheaths (fascia) and basement membranes. Matrix Biol. 28:32–43.

Bédécarrats, G. Y., M. Baxter, and B. Sparling. 2016. An updated model to describe the neuroendocrine control of reproduction in chickens. Gen. Comp. Endocrinol. 227:58–63.

Buckland, R., and G. Guy. 2002. Breeder flock management. Goose production. Food and Agricultural Organization of the Unitednations, Rome.

Button, R. W., S. L. Roberts, T. L. Willis, C. O. Hanemann, and S. Luo. 2017. Accumulation of autophagosomes confers cytotoxicity. J. Biol. Chem. 292:13599–13614.

Cetica, P. 2002. Activity of key enzymes involved in glucose and triglyceride catabolism during bovine oocyte maturation in vitro. Reproduction 124:675–681.

Chen, C. P., S. H. Liu, M. Y. Lee, and Y. Y. Chen. 2008. Heparan sulfate proteoglycans in the basement membranes of the human placenta and decidua. Placenta 29:309–316.

Chen, S. Y., W. H. Chen, J. Yu, F. F. Yan, and A. Y. Zhao. 2020. Effects of light on laying and nest-related behavior of zhedong white geese, *Chin. J. Anim. Sci.*, **57**, 2021, 243-247.

Cheng, L. 2018. Study on the changes of microenvironmental metabolism and antioxidant levels in porcine healthy and atretic follicles. Master. Nanjing Agricultural University, China.

Choi, J., M. Jo, E. Lee, and D. Choi. 2011. Induction of apoptotic cell death via accumulation of autophagosomes in rat granulosa cells. Fertil. Steril. 95:1482–1486.

Choi, J. Y., M. W. Jo, E. Y. Lee, B.-K. Yoon, and D. S. Choi. 2010. The role of autophagy in follicular development and atresia in rat granulosa cells. Fertil. Steril. 93:2532–2537.

Del Pozo Martin, Y., D. Park, A. Ramachandran, L. Ombrato, F. Calvo, P. Chakravarty, B. Spencer-Dene, S. Derzsi, C. S. Hill, E. Sahai, and I. Malanchi. 2015. Mesenchymal cancer cell-stroma crosstalk promotes niche activation, epithelial reversion, and metastatic colonization. Cell Rep. 13:2456–2469.

Deviche, P., C. Saldanha, and R. Silver. 2000. Changes in brain gonadotropin-releasing hormone- and vasoactive intestinal polypeptide-like immunoreactivity accompanying reestablishment of photosensitivity in male dark-eyed juncos (Junco hyemalis). Gen. Comp. Endocrinol. 117:8–19.

Du, P. 2018. mir-1246 knockdown via lentivirus inhibits tumor growth and promotes apoptosis of cervical cancer cells by targeting thrombospondin-2. PhD. Guangxi Medical Univerisity, China.

Flück, M., V. Tunc-Civelek, and M. Chiquet. 2000. Rapid and reciprocal regulation of tenascin-C and tenascin-Y expression by loading of skeletal muscle. J. Cell Sci. 113:3583–3591.

Gannon, A. M., M. R. Stämpfli, and W. G. Foster. 2012. Cigarette smoke exposure leads to follicle loss via an alternative ovarian cell death pathway in a mouse model. Toxicol. Sci. 125:274–284.

Gómez-Sánchez, R., S. A. Tooze, and F. Reggiori. 2021. Membrane supply and remodeling during autophagosome biogenesis. Curr. Opin. Cell Biol. 71:112–119.

Grindel, B. J., J. R. Martinez, C. L. Pennington, M. Muldoon, J. Stave, L. W. Chung, and M. C. Farach-Carson. 2014. Matrilysin/matrix metalloproteinase-7(MMP7) cleavage of perlecan/HSPG2 creates a molecular switch to alter prostate cancer cell behavior. Matrix Biol. 36:64–76.

Gustafsson, E., M. Almonte-Becerril, W. Bloch, and M. Costell. 2013. Perlecan maintains microvessel integrity in vivo and modulates their formation in vitro. PLoS One 8:e53715.

Homa, S., C. Racowsky, and R. McGaughey. 1986. Lipid analysis of immature pig oocytes. J. Reprod. Fertil. 77:425–434.

Hong, F., G. L. Yuan, H. J. Zhang, K. Liu, S. A. Cheng, X. X. Peng, and Z. R. Gu. 2017. Expression and clinical implications of Stathmin and CD133 in osteosarcoma. Chin. J. Exp. Surg. 34:516–518.

Howard, M. J., and C. M. Isacke. 2002. The C-type lectin receptor Endo180 displays internalization and recycling properties distinct from other members of the mannose receptor family*. J. Biol. Chem. 277:32320–32331.

Inoue, N., F. Matsuda, Y. Goto, and N. Manabe. 2011. Role of cell-death ligand-receptor system of granulosa cells in selective follicular atresia in porcine ovary. J. Reprod. Dev. 57:169–175.

Iozzo, R. V., I. R. Cohen, S. Grässel, and A. D. Murdoch. 1994. The biology of perlecan: the multifaceted heparan sulphate proteoglycan of basement membranes and pericellular matrices. Biochem. J. 302:625–639.

Jing, R., L. Gu, J. Li, and Y. Gong. 2018. A transcriptomic comparison of theca and granulosa cells in chicken and cattle follicles reveals ESR2 as a potential regulator of CYP19A1 expression in the theca cells of chicken follicles. Comp. Biochem. Physiol. D Genomics Proteomics 27:40–53.

Kabeya, Y., N. Mizushima, T. Ueno, A. Yamamoto, T. Kirisako, T. Noda, E. Kominami, Y. Ohsumi, and T. Yoshimori. 2000. LC3, a mammalian homologue of yeast APG8P, is localized in autophagosome membranes after processing. EMBO J. 19:5720–5728.

Klionsky, D. J. 2005. Autophagy. Curr. Biol. 15:R282–R283.

Leska, A., and L. Dusza. 2007. Seasonal changes in the hypothalamo-pituitary-gonadal axis in birds. Reprod. Biol. 7:99–126.

Lin, P., and R. Rui. 2010. Effects of follicular size and FSH on granulosa cell apoptosis and atresia in porcine antral follicles. Mol. Reprod. Dev 77:670–678.

Lockshin, R., and Z. Zakeri. 2005. Apoptosis, autophagy, and more. Int. J. Biochem. Cell Biol. 36:2405–2419.

Lou, Y., W. Yu, L. Han, S. Yang, Y. Wang, T. Ren, J. Yu, and A. Zhao. 2017. ROS activates autophagy in follicular granulosa cells via mTOR pathway to regulate broodiness in goose. Anim. Reprod. Sci. 185:97–103.

Lu, C., J. Zhang, S. He, C. Wan, A. Shan, Y. Wang, L. Yu, G. Liu, K. Chen, J. Shi, Y. Zhang, and R. Ni. 2013. Increased α-tubulin1b expression indicates poor prognosis and resistance to chemotherapy in hepatocellular carcinoma. Dig. Dis. Sci. 58:2713–2720.

Ma, H.-P., H.-L. Chang, O. A. Bamodu, V. Yadav, T.-Y. Huang, A. wu, C.-T. Yeh, S.-H. Tsai, and W.-H. Lee. 2019. Collagen 1A1 (COL1A1) is a reliable biomarker and putative therapeutic target for hepatocellular carcinogenesis and metastasis. Cancers 11:786.

Madsen, D., H. Jürgensen, S. Z. Ingvarsen, M. Melander, B. Vainer, K. Egerod, A. Hald, B. Rønø, C. Madsen, T. Bugge, L. Engelholm, and N. Behrendt. 2012. Endocytic collagen degradation: a novel mechanism involved in protection against liver fibrosis. J. Pathol. 227:94–105.

Markström, E., E. F. Svensson, R. Shao, B. Svanberg, and H. Billig. 2002. Survival factors regulating ovarian apoptosis – dependence on follicle differentiation. Reproduction 123:23–30.

Matsuda, F., N. Inoue, N. Manabe, and S. Ohkura. 2012. Follicular growth and atresia in mammalian ovaries: regulation by survival and death of granulosa cells. J. Reprod. Dev. 58:44–50.

Mauro, L., O. Youngren, J. Proudman, R. Phillips, and M. El Halawani. 1992. Effects of reproductive status, ovariectomy, and photoperiod on vasoactive intestinal peptide in the female turkey hypothalamus. Gen. Comp. Endocrinol. 87:481–493.

Mishra, M., V. Naik, A. Kale, A. Ankola, and G. Pilli. 2011. Perlecan (basement membrane heparan sulfate proteoglycan) and its role in oral malignancies: an overview. Indian J Dental Res 22:823–826.

Morais, R. D. V. S., R. G. Thomé, F. S. Lemos, N. Bazzoli, and E. Rizzo. 2012. Autophagy and apoptosis interplay during follicular atresia in fish ovary: a morphological and immunocytochemical study. Cell Tissue Res. 347:467–478.

Nakane, Y., K. Ikegami, H. Ono, N. Yamamoto, S. Yoshida, K. Hirunagi, S. Ebihara, Y. Kubo, and T. Yoshimura. 2010. A mammalian neural tissue opsin (Opsin 5) is a deep brain photoreceptor in birds. Proc. Natl. Acad. Sci. U.S.A. 107:15264–15268.

Nishiyama, T., A. M. McDonough, R. R. Bruns, and R. E. Burgeson. 1994. Type XII and XIV collagens mediate interactions between banded collagen fibers in vitro and may modulate extracellular matrix deformability. J. Biol. Chem. 269:28193–28199.

Pearce, O., R. Delaine-Smith, E. Maniati, S. Nichols, J. Wang, S. Böhm, V. Rajeeve, D. Ullah, P. Chakravarty, R. Jones, A. Montfort, T. Dowe, J. Gribben, J. Jones, H. Kocher, J. Serody, B. Vincent, J. Connelly, J. Brenton, and F. Balkwill. 2017. Deconstruction of a metastatic tumor microenvironment reveals a common matrix response in human cancers. Cancer Discov. 8:CD–17.

Raglow, Z., and S. M. Thomas. 2015. Tumor matrix protein collagen XIα1 in cancer. Cancer Lett. 357:448–453.

Rowan, W. 1925. Relation of light to bird migration and developmental changes. Nature 115:494–495.

Santos, H., R. Thomé, F. Arantes, Y. Sato, N. Bazzoli, and E. Rizzo. 2008. Ovarian follicular atresia is mediated by heterophagy, autophagy, and apoptosis in Prochilodus argenteus and Leporinus taeniatus (Teleostei: Characiformes). Theriogenology 70:1449–1460.

Shi, Z. D., Y. M. Huang, A. D. Sun, and S. D. Liang. 2005. Study on photoperiodic regulation of reproductive seasonality of Guandong greylag geese Guangdong. Agric. Sci. 3:72–75.

Shi, Z. D., Y. B. Tian, W. Wu, and Z. Y. Wang. 2008. Controlling reproductive seasonality in the geese: a review. Worlds Poult. Sci. J. 64:343–355.

Stolz, A., A. Ernst, and I. Dikic. 2014. Cargo recognition and trafficking in selective autophagy. Nat. Cell Biol. 16:495–501.

Sturmey, R. G., A. Reis, H. J. Leese, and T. G. McEvoy. 2009. Role of fatty acids in energy provision during oocyte maturation and early embryo development. Reprod. Domest. Anim. 44:50–58.

Tilly, J., K. Kowalski, A. Johnson, and A. Hsueh. 1991. Involvement of apoptosis in ovarian follicular atresia and posovulatory regression. Endocrinology 129:2799–2801.

Trächslin, J., M. Koch, and M. Chiquet. 1999. Rapid and reversible regulation of collagen XII expression by changes in tensile stress. Exp. Cell. Res. 247:320–328.

Vázquez, F., M. García-Ocaña, J. Galván, J. Martínez, C. García-Pravia, P. Menéndez, C.-d. Rey, L. Barneo, and J. Toyos. 2015. COL11A1/(pro)collagen 11A1 expression is a remarkable biomarker of human invasive carcinoma-associated stromal cells and carcinoma progression. Tumor Biol 36:1–10.

Winkler, S., R. Stahl, D. Carey, and R. Bansal. 2002. Syndecan-3 and perlecan are differentially expressed by progenitors and mature oligodendrocytes. J. Neurosci. Res. 69:477–487.

Wu, J., Y. Dang, W. Su, C. Liu, H. Ma, Y. Shan, Y. Pei, B. Wan, J. Guo, and L. Yu. 2006. Molecular cloning and characterization of rat LC3A and LC3B—two novel markers of autophagosome. Biochem. Biophys. Res. Commun. 339:437–442.

Xie, Z., and D. J. Klionsky. 2007. Autophagosome formation: core machinery and adaptations. Nat. Cell Biol. 9:1102–1109.

Yamashita, T., H. Ohuchi, S. Tomonari, K. Ikeda, K. Sakai, and Y. Shichida. 2010. Opn5 is a UV-sensitive bistable pigment that couples with Gi subtype of G protein. Proc. Nat. Acad. Sci. U.S.A. 107:22084–22089.

Yin, Y. F., Q. H. Hu, Y. C. Du, W. G. Fu, and X. M. Xia. 2021. Role of extracellular matrix in the occurrence and development of hepatocellular carcinoma. Chin J. Gen. Surg. 30:91–97.

Yoshimura, T. 2013. Thyroid hormone and seasonal regulation of reproduction. Front. Neuroendocrinol. 34:157–166.

Zhang, J., Y. Xu, H. Liu, and Z. Pan. 2019. MicroRNAs in ovarian follicular atresia and granulosa cell apoptosis. Reprod. Biol. Endocrinol. 17:9.

Zhao, W., T. Yuan, Y. Fu, D. Niu, W. Chen, L. Chen, and L. Lu. 2020. Seasonal differences in the transcriptome profile of the Zhedong white goose (Anser cygnoides) pituitary gland. Poult. Sci. 100:1154–1166.

Zhao, X., T. Shao, Y. Wang, X. Lu, J. Luo, and W. Zhou. 2013. The phytoestrogen daidzein may affect reproductive performance of Zhedong White geese by regulating gene mRNA levels in the HPG axis. Br. Poult. Sci. 54:252–258.

Zhao, Y., P. Codogno, and H. Zhang. 2021. Machinery, regulation and pathophysiological implications of autophagosome maturation. Nat. Rev. Mol. Cell Biol. 22:733–750.

Zhou, J., X. Peng, and S. Mei. 2019. Autophagy in ovarian follicular development and atresia. Int. J. Biol. Sci 15:726–737.